Clinical and Experimental Immunology, 2023, **214**, 36–49
https://doi.org/10.1093/cei/uxad073
Advance access publication 9 July 2023
Research Article

Clinical & Experimental IMMUNOLOGY

OXFORD

Research Article

Dissecting T-cell heterogeneity in esophageal squamous cell carcinoma reveals the potential role of LAIR2 in antitumor immunity

Ping Wang[1,2,‡], Weitao Zhuang[3,‡], Zhuojun Zheng[2], Liyun Zhang[2], Xu Zhang[4,*] and Qingyun Chen[1,*]

[1]Medical Research Institute, Guangdong Provincial People's Hospital (Guangdong Academy of Medical Sciences), Southern Medical University, Guangzhou, Guangdong, China
[2]Department of Immunology, School of Basic Medical Sciences, Southern Medical University, Guangzhou, Guangdong, China
[3]Department of Medical Oncology, State Key Laboratory of Oncology in South China, Collaborative Innovation Center for Cancer Medicine, Sun Yat-sen University Cancer Center, Guangzhou, Guangdong, China
[4]Department of Medical Oncology, State Key Laboratory of Oncology in South China, Sun Yat-sen University Cancer Center, Guangzhou, Guangdong, China

[*]Correspondence: Qingyun Chen, Medical Research Institute, Guangdong Provincial People's Hospital (Guangdong Academy of Medical Sciences), Southern Medical University, Guangzhou, Guangdong, China. Email: chenqingyun@gdph.org.cn; Xu Zhang, Department of Medical Oncology, State Key Laboratory of Oncology in South China, Sun Yat-sen University Cancer Center, Guangzhou, Guangdong, China. Email: zhangxu@sysucc.org.cn
[‡]These authors have contributed equally to this work and share first authorship.

Abstract

Esophageal squamous cell carcinoma (ESCC), one of the most commonly diagnosed and lethal malignant diseases, has a complex tumor ecosystem. An obvious requirement for T-cell-mediated tumor control is the infiltration of tumor-reactive T cells into the tumor. Here, we obtained detailed T-cell compositions in both ESCC tumors and matched peripheral blood mononuclear cells (PBMCs) at single-cell resolution. We demonstrated that T cells in tumors and PBMCs had different compositions and functional states. ESCC tumors were rich in Treg and exhausted T cells but poor in cytotoxic and naïve T cells compared with PBMCs. The exhausted T cells showed higher exhausted signature in tumors than in PBMCs, while the cytotoxic T cells exhibited higher cytotoxic signature in PBMCs than in tumors. Our data indicated an immunosuppressive status and a defect at the level of T-cell priming in the tumor microenvironment. Leukocyte-associated Ig-like receptor-2 (LAIR2), a soluble collagen receptor that prevents the binding of human leukocyte-associated Ig-like receptor-1 (LAIR1) to collagens, was predominantly expressed in proliferating $CD8^+$ T and Treg cells in tumors but in cytotoxic cells in PBMCs. LAIR2 could inhibit tumor metastasis, invasion, and collagen deposition via suppressing transforming growth factor-β signaling. These findings revealed differential T-cell populations in tumors and PBMCs and provided convincing evidence that LAIR2 acted as a tumor suppressor.

Keywords: esophageal cancer, single-cell RNA sequencing, LAIR2, tumor metastasis

Abbreviations: EMT: epithelial-mesenchymal transition; ESCC: esophageal squamous cell carcinoma; F-actin: fibrillar actin; G-actin: globular actin; GSEA: gene set enrichment analysis; LAIR1: leukocyte-associated Ig-like receptor-1; LAIR2: leukocyte-associated Ig-like receptor-2; PBMCs: peripheral blood mononuclear cells; TME: tumor microenvironment.

Introduction

Esophageal cancer is one of the most commonly diagnosed and deadly cancer types and seriously threatens human health. Histologically, esophageal cancer can be classified into two subtypes: adenocarcinoma (EAC) and squamous cell carcinoma (ESCC). ESCC makes up ~90% of esophageal cancer cases in East Asia [1]. ESCC has a poor prognosis with a 5-year survival rate of around 15–25%, probably due to the difficulty in early diagnosis and its inherent resistance to chemotherapy [2, 3]. Currently, promising immunotherapy for ESCC treatment is gaining attention. Although pembrolizumab is approved by the US Food and Drug Administration (FDA) to treat patients who have progressed after second-line therapies, this anti-PD-1 antibody did not significantly improve overall survival compared with paclitaxel therapy for advanced gastric or gastro-esophageal junction cancer whose tumors are PD-L1 positive [4]. To improve ESCC immunotherapy's efficacy and to develop novel biomarkers to facilitate ESCC prognosis prediction, a recent study discovered 42 cell types, including 26 immune cell subtypes and 16 nonimmune stromal cell subpopulations in the tumor microenvironment (TME) [5]. Herein, we focused on T-cell populations, which were the main immune therapy targets of ESCC immune treatment.

Received 11 September 2022; Revised 4 May 2023; Accepted for publication 3 July 2023

Leukocyte-associated Ig-like receptor-1 (LAIR1) is a member of the Ig superfamily. Antibody-induced cross-linking of the receptor *in vitro* delivers a strong inhibitory signal. This inhibitory signal is dependent on the phosphorylation of tyrosine-based inhibitory motifs (ITIMs) located at the cytoplasmic tail of LAIR1 [6]. Collagens present the most abundant type of proteins in the extracellular matrix in tumors, and overexpression of collagens has been associated with poor overall survival in many tumor types [7]. Cross-linking of LAIR1 with collagens delivers a potent inhibitory signal that is capable of suppressing the function and/or differentiation of NK cells [8], T cells [9], B cells [10], dendritic cells, and monocytes [11]. Thus, the interaction of LAIR1 with collagens in the TME may represent a novel mechanism to promote immune evasion [12].

LAIR2 is a natural soluble homolog of LAIR1 that shares ~84% identity with the LAIR1 extracellular region but lacks the intracellular and transmembrane domains. LAIR2 binds to collagens with a higher affinity than LAIR1 and prevents the binding of human LAIR1 to collagens and LAIR1 cross-linking *in vitro* [13]. Targeting LAIR1 signaling through LAIR2 overexpression or SHP-1 inhibition sensitizes resistant tumors to PD-1 blockade and markedly reduces tumor growth and metastasis [14]. Circulating LAIR2 protein concentration was low or undetectable in healthy individuals [15]. Increased LAIR2 level was observed in synovial fluid of patients with rheumatoid arthritis and ankylosing spondylitis, suggesting that LAIR2 expression was associated with increased inflammation [13, 16]. LAIR2 may function as a proinflammatory mediator by decreasing the inhibitory activity of immune suppressor LAIR1, leading to a more highly activated immune response. For example, a recent study found that a dimeric LAIR2 Fc fusion protein-NC410 significantly promoted T-cell-mediated antitumor immunity in the humanized tumor model [15]. However, another study indicated that LAIR2 was preferentially expressed by regulatory T cells (Tregs), and LAIR2 expression was adversely prognostic in lung adenocarcinoma [17]. Therefore, although LAIR2 is an essential component of cancer regulation, its role in antitumor immunity needs further investigation.

In the present study, we have performed single-cell RNA sequencing (scRNA-seq) on T cells derived from ESCC tumors and matched peripheral blood mononuclear cells (PBMCs) obtained from eight patients to decode the transcriptome alterations between tumors and PBMCs. By analyzing these results, we have established a landscape of T cells in ESCC tumors and PBMCs. After clarifying the expression pattern of LAIR2 in T cells at the single-cell resolution, we performed *in vitro* and *in vivo* experiments to study its biological function against tumors.

Materials and methods

Human specimens

Human tumor tissues and PBMCs for scRNA-seq were obtained with informed written consent for five male patients and three female patients with ESCC who underwent surgery at the Sun Yat-sen University Cancer Center (Guangzhou, Guangdong, PR China). The patients' information was shows in Supplementary Fig. 2d. None of these patients were treated with chemotherapy or radiation prior to tumor resection. The collection of all the samples used in this study were approved by the Committees for the Ethical Review of Research Involving Human Subjects at the Sun Yat-sen University Cancer Center (Guangzhou, Guangdong, PR China).

scRNA-seq data processing

Cell Range Software provided by 10 × genomics was used to decode the cellular barcodes, map reads to the genome, and transcriptome. This output was then imported into the Seurat (v3) T toolkit for quality control and downstream analysis. All functions were ran with default parameters. To remove the batch effector, the datasets collected from different samples were integrated using Seurat v3 with default parameters.

Dimensionality reduction, clustering, and annotation

The Seurat function "Find Variable Features" was applied to identify the highly variable genes (HVGs). The top 2000 HVGs were used for data integration. The data were scaled using "Scale Data," and the first 20 principal components were adopted for autoclustering analyses using "Find Neighbors" and "Find Clusters" functions. For all cells, we identified clusters setting the resolution parameter as 0.8, and the clustering results were visualized with the UMAP scatter plot. The marker genes of each cell cluster were identified using the Seurat "Find All Markers" function for top genes. We used the Cluster Profiler and GSEA packages to perform enrichment analysis on the differentially expressed genes in each cluster or subset. We used published signature gene lists that have been previously described for cytotoxicity, exhaustion, Treg, and naïve scores [18].

Cell line and cell culture condition

The human esophageal cell line KYSE150 was cultured in 1640 medium (Gibco, USA) supplemented with 10% fetal bovine serum (Serana, Germany), 100 U/mL penicillin, and 100 mg/mL streptomycin (Invitrogen, USA) at 37°C in 5% CO_2. The culture media was replaced every 2 to 3 days, and the logarithmic phase cells were used for the following experiments.

Cell growth and foci formation assays

CCK-8 assay and colony formation assay were utilized to evaluate cells proliferation. For CCK-8 assay, cells were seeded at a density of 1000 per well in 96-well plates. The cell growth rate was monitored using a CCK-8 assay kit (Dojindo, Japan) according to the manufacturer's instructions. For foci formation assay, 1000 cells were seeded in six-well plates and cultured for 14 days prior to 4% paraformaldehyde fixation and 0.1% crystal violet staining.

Wound healing assay

For wound healing assay, a total of 6×10^5 cells were grown as a confluent monolayer in six-well plates and treated with or without LAIR2 (Human, R&D Systems, USA)/transforming growth factor-β (TGF-β1) (Human, Sinobiological, China). Upon the cells reaching ~90% confluence, the cells in the monolayer were vertically scratched using a 200 μl pipet tip. Subsequently, floating cells were carefully removed with PBS before adding the fresh medium. The wound healing process was monitored under an inverted light microscope. The migration abilities were quantified and normalized by the relative gap distance.

Cell migration, chemotaxis, invasion assays

Cell motility was additionally assessed by cell migration and invasion arrays using transwell chambers (Corning, USA) with a pore size of 8 μm. For the migration assay, after serum starvation for 24 hours, 1×10^5 KYSE150 cells in serum-free medium were layered in the upper chamber, and the medium containing 20% FBS was applied to the lower chamber. A gradient concentration of CXCL12 (Human, Abclonal, China) were added in the lower chamber of transwells for chemotaxis assay, with or without LAIR2 in upper chamber. For the invasion assay, a total of 3×10^5 cells were plated in the serum-free medium in the upper chamber of a matrigel-coated transwell after starvation with or without LAIR2. The chamber was then incubated for 48 hours at 37°C. After removing the cells in the upper surface of the filter with a cotton swab, the invasive cells attached to the lower surface of the membrane were fixed with 4% paraformaldehyde followed by staining with 0.1% crystal violet, and then quantified by counting the cell number at six random fields under a microscope.

Regents

The antibodies of Smad2/3 (3102, CST), AKT (#9272, CST), p-AKT (#9271, CST), p-Smad2/3 (#ab272332, Abcam), E-cadherin (#20874-1-AP, Proteintech), N-cadherin (#22018-1-AP, Proteintech), Vimentin (#BF8006, Affinity Biosciences), Collagen Type I (#14695-1-AP, Proteintech), NF-κB1 (#14220-1-AP, Proteintech), LEF-1 (#28540-1-AP, Proteintech), PD-L1 (#66248-1-Ig, Proteintech), GAPDH (#60004-1-Ig, Proteintech), SNAIL (#AF6032, Affinity Biosciences), ROCK1 (#PTM-6454, PTM Bio), ROCK2 (#PTM-6169, PTM Bio), Ki67 (#GB111499, Servicebio), and fibrillar actin (F-actin) (#C1033, Beyotime) were used for western blot, immunofluorescence staining, and immunohistochemical staining. The following antihuman antibodies were used for flow cytometry: CD45 (PE, 30-F11; eBioscience), CD8α (APC, 53–6.7; eBioscience), 7-AAD (Invitrogen), CD3 (eFluor™ 506, UCHT1; eBioscience), PD-1 (Pacific Blue, EH12.2H7; Biolegend), and TIM-3 (FITC, F38-2E2; Biolegend).

Western blotting assay analysis

The cells were homogenized in RIPA buffer containing protease inhibitor (Beyotime Institute of Biotechnology, China). BCA protein assay kit (Beyotime Institute of Biotechnology) was used to measure protein concentrations. The cell extracts were resolved by SDS-PAGE and transferred onto polyvinylidene fluoride membranes (Millipore, USA). After blocking with 5% bovine serum albumin (BSA) in Tris-buffered saline containing 0.05% Tween 20, the membranes were then incubated with the specific primary antibodies. Following incubation with corresponding HRP-conjugated secondary antibody (Proteintech, USA), the target proteins were visualized with enhanced chemiluminescence (Thermo Fisher, USA). The intensity of the protein band was evaluated using ImageJ software, and the relative protein levels were normalized to GAPDH.

Quantitative real-time PCR analysis

Total RNA isolation was performed using TRIzol reagent (TransGene Biotech, China). A total of 1 μg of total RNA was reverse transcribed using TranScript All-in-One First-Strand cDNA Synthesis SuperMix (TransGene Biotech) according to the instructions of the manufacturer. Real-time PCR was performed with an Eppendorf Realplex PCR system using TransStart Tip Green qPCR SuperMix (TransGene Biotech). Primers used in the qPCR reactions, which were all from PrimerBank (Wang *et al.*, 2012) and synthesized by Huada Gene Technology Co., Ltd. (Shenzhen, China), were presented in Table 1.

Flow cytometry

PBMCs were isolated and cultured with 1 μg/mL of anti-CD3 and anti-CD28 antibody (Invitrogen) for 48 hours. Tumor cells were seeded 24 hours before the endpoint of PBMCs activation. PBMCs were added to the tumor cells at a 4:1 ratio and cocultured for 48 hours with or without LAIR2. Culture supernatant, which mainly composed of PBMCs and adherent cells that were mainly tumor cells, were separately collected, stained, and analyzed in flow cytometry.

Immunofluorescence staining

A total of 1×10^4 KYSE150 cells were seeded on confocal dishes overnight and treated with or without LAIR2/CXCL12 for 48 hours. The cells were fixed with 4% paraformaldehyde for 15 minutes, washed with PBS, and then permeabilized for 30 minutes with PBS containing 0.5% Triton X-100. Subsequently, the cells were blocked with 4% BSA at room temperature for 1 hour and incubated with F-actin overnight at 4°C. Thereafter, the sections were stained with 0.5 μg/ml DAPI for 5 minutes and visualized with confocal microscopy. The mean fluorescence intensity was measured by ImageJ software.

Animal experiments

BALC/c nude mice (male, 5 weeks old) were purchased from the Guangdong Medical Laboratory Animal Center (Guangzhou, China). The mice were maintained under a 12-hour light/dark cycle in a specific pathogen-free condition

Table 1. Primers used for real-time PCR in this study

Gene	Forward (5′–3′)	Reverse (5′–3′)
E-cadherin	CGAGAGCTACACGTTCACGG	GGGTGTCGAGGGAAAAATAGG
N-cadherin	TGCGGTACAGTGTAACTGGG	GAAACCGGGCTATCTGCTCG
Vimentin	GATGTTTCCAAGCCTGACCT	CACTTCACAGGTGAGGGACT
SLUG	CGAACTGGACACACATACAGTG	CTGAGGATCTCTGGTTGTGGT
TWIST1	GTCCGCAGTCTTACGAGGAG	GCTTGAGGGTCTGAATCTTGCT
COL1A1	GAGGGCCAAGACGAAGACATC	CAGATCACGTCATCGCACAAC
GAPDH	GGAGCGAGATCCCTCCAAAAT	GGCTGTTGTCATACTTCTCATGG

with a controlled temperature (20–25°C) and humidity (50 ± 5%). After being intravenously injected with 1×10^6 KYSE150 cells via the tail vein, the mice were randomly divided into two groups, receiving an intraperitoneal injection of 6 μg/kg LAIR2 or PBS for 4 weeks (n = 10). Weights of mice were recorded.

Histopathological and immunohistochemical staining

After treatment for 28 days, the mice were sacrificed, and the lungs were immediately removed, fixed, embedded in paraffin, and sectioned into 4 μm slices. Then, the slices were stained with Hematoxylin and Eosin Staining Kit (Servicebio, China) and Masson's Trichrome Staining Kit (Servicebio), respectively, according to the manufacturer's instructions. For immunohistochemical staining, the sections were deparaffinized and soaked with 3% H_2O_2 for 10 minutes. Antigen repair was performed with antigen retrieval buffer (ZSbio, China). Then, the sections were blocked with 4% BSA at room temperature for 30 minutes, followed by incubating with diluted antibody at 4°C overnight. After washing with PBS, the sections were incubated with a second antibody at room temperature for another 1 hour, then stained with DAB kit (Beyotime, China) and hematoxylin (Servicebio), and visualized under microscope. The positive cells and collagen volume fraction were calculated by the ImageJ software.

Statistical analysis

All data are presented as the mean ± SD. Statistical analyses were performed using SPSS 21.0 software. Comparisons between four groups were determined by one-way ANOVA or Kruskal–Wallis test, and multiple comparisons were done. Data from two groups were compared with non-paired t-test or Mann Whitney U test. Differences were considered to be statistically significant at $P < 0.05$.

Results

scRNA-seq resolves T-cell types in ESCC patients

To characterize the T-cell subtypes in ESCC patients, we performed droplet-based scRNA-seq to study the transcriptomic profiles of T cells in TME and PBMCs. We sorted $CD3^+$ $CD4^+$ and $CD3^+$ $CD8^+$ T cells from single-cell suspensions prepared from tumors and corresponding peripheral blood of eight ESCC patients. Single-cell transcriptome data were acquired from 8723 and 7815 T cells in tumors and PBMCs, respectively. After preprocessing, normalization, and batch correction, unsupervised clustering was performed on 16 538 T cells. We applied principal component analysis across all cells and identified 15 T-cell clusters (Fig. 1a and b, Supplementary Fig. 1a). The compositions of each cluster in tumors and corresponding PBMCs were shown in Fig. 1c and Supplementary Fig. 1b and c. C2, C4, C6, and C10 clusters with both $CD4^+$ and $CD8^+$ T cells carried a naive signature, including SELL, CCR7, and TCF7, and expressed very low levels of cytokines and effective genes. Therefore, these groups of cells were collectively named naïve T cells [19]. C5-IL7R cluster that had both $CD4^+$ and $CD8^+$ T cells shared a few common genes with naïve T cells but also highly expressed IL7R, KLF2, and ANXA1, suggesting a central memory T-cell phenotype [20]. Other T-cell subsets, according to cell lineage and expression of signature genes, were identified as C7-CD4-FOXP3 Treg cells, C0-CD8-Tex exhausted T cells, C12-CD8-IFIT3 interferon-related T cells, and C14-CD8-STMN1 proliferating T cells (Fig. 1d and f). C1-CD8-GZMK, C3-CD8-FGFBP2, C11-CD8-KLRG1, and C8-CD8-ZNF683 T cells were hierarchically clustered together. They expressed different levels of effector molecules, such as NKG7, GZMA, PRF1, and GNLY (Fig. 1e–g), indicating these T cells were effector memory or cytotoxic $CD8^+$ T cells. C9 T cells had upregulation of mitochondrial transcripts and lower total UMI counts (Supplementary Fig. 1d), likely representing a population of dead or dying cells. C13 cells were macrophages that express known markers, such as CD68, LYZ, CD14, and FCER1G (Supplementary Fig. 1e). We excluded these two clusters in the following analysis.

To reveal the differences in T-cell composition between ESCC tumors and PBMCs, we calculated the percentages of the 10 main T-cell types in tumors and PBMCs. Naïve T cells were the most abundant T cells in PBMCs, making up ~48% of the total T cells, while they were only 18% in tumors. The most abundant T cells in the tumors were C0-CD8-Tex cells, making up ~28% of the total T cells in tumors, but only 2% in PBMCs. C12-CD8-IFIT3 interferon-related $CD8^+$ T cells, C14-CD8-STMN1 proliferating $CD8^+$ T cells, and Treg cells were highly enriched in tumors rather than in PBMCs. In contrast, the proportions of C3-CD8-FGFBP2 and C11-CD8-KLRG1 cytotoxic $CD8^+$ T cells accounted for 15% and 5%, respectively, in PBMCs, while 8% and <1% in tumors, indicating that cytotoxic $CD8^+$ T cells accumulated in larger numbers in PBMCs compared with tumors. Other T cells, including C1-CD8-GZMK, C8-CD8-ZNF683 T cells, and C5-IL7R central memory T cells, showed comparable percentages between tumors and PBMCs (Fig. 2a). We also calculated the relative frequencies of individual T-cell subtypes that constituted the sample origins, namely, tumors and PBMCs. It was revealed that C0-CD8-Tex, C12-CD8-IFIT3, C14-CD8-STMN1, and Treg cells were predominantly derived from tumors rather than PBMCs. On the contrary, the majority of C11-CD8-KLRG1 and naïve T cells originated from PBMCs rather than tumors (Fig. 2b). These data suggested that ESCC tumors were rich in Tregs and exhausted T cells but poor in cytotoxic and naïve T cells compared with PBMCs, indicating an immunosuppressive status in the TME.

To investigate gene expression profiles in cytotoxic, exhausted, naïve, and Treg cells, we used the public naïve, Treg, exhaustion, and cytotoxic signatures [21] to calculate scores and quantify the properties of each cell type. We found that C7-CD4-FOXP3 Treg cells had the strongest Treg signature, while C0-CD8-Tex had the most robust exhaustion signature, followed by C14-CD8-STMN1 T cells (Fig. 3a). C3-CD8-FGFBP2 was the most active cytotoxic $CD8^+$ T-cell type. Genes in the "naive" signature were dramatically enriched in naïve T cells (Fig. 3a). We further compared the signatures for cytotoxicity, exhaustion, naïve, and Treg in each T-cell cluster between tumors and PBMCs (Fig. 3b). C7-Treg cells showed higher Treg signature genes in tumors than those in PBMCs. In contrast, the naïve score of naïve T cells was much higher in PBMCs than tumors (Fig. 3b). Interestingly, although C3-CD8-FGFBP2 accounted for a comparable proportion of T cells in tumors and PBMCs (Fig. 2b), the cytotoxic score of C3-CD8-FGFBP2 was much higher in PBMCs than that in tumors (Fig. 3b, dashed box), indicating the immune suppressive environment or a defect

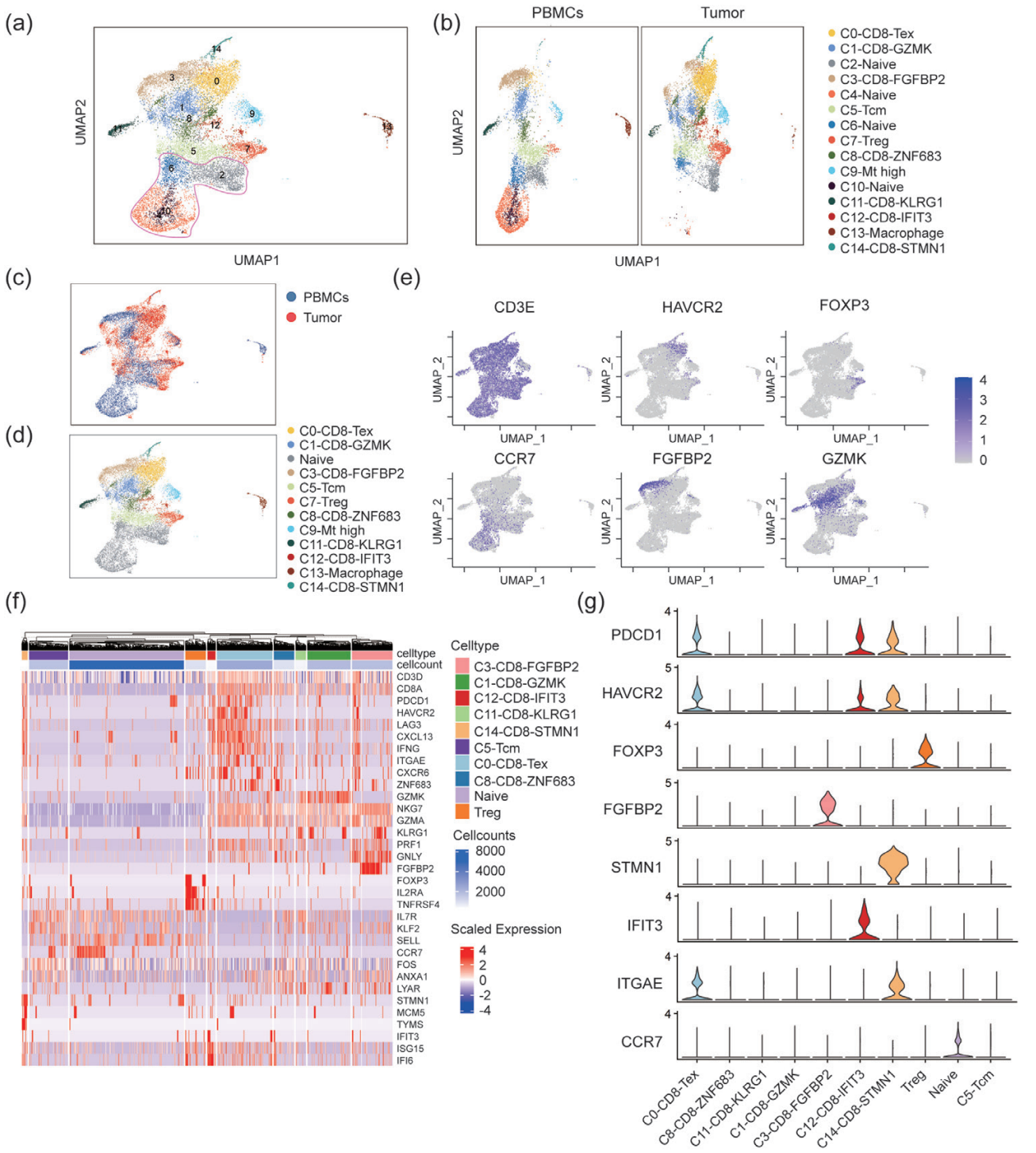

Figure 1. Profiles of T-cell clusters in human ESCC tumors and PBMCs with scRNA-seq. (a–c) UMPA plot showing the T-cell types based on the expression of known marker genes in tumors and PBMCs, colored according to cell types. (d) Expression levels of relative maker genes across 16 538 cells illustrated as UMAP plots. (e) Heatmap of the relative expression level of genes across cells, sorted by cell type. The expression was measures as the *z*-score normalized $\log_2$(count + 1). (f) Violin plot showing the PDCD1, HAVCR2, FOXP3, FGFBP2, STMN1, IFIT3, ITGAE, and CCR7 in main T-cell clusters.

at the level of T-cell priming in the tumor. Notably, both C0-CD8-Tex and C14-CD8-STMN1 T cells demonstrated opposite gene-expressing profiles in tumors and PBMCs. They showed higher exhausted signatures in tumors, while exhibited higher cytotoxic signatures in PBMCs (Fig. 3b, dashed box). Besides, C0-CD8-Tex and C14-CD8-STMN1 T cells were likely tumor-reactive T cells because of high levels of CD39 (ENTPD1) and CD103 (ITGAE) and deficient level of KLRG1 (Fig. 3c) [22]. Different stages of $CD8^+$ T-cell exhaustion have been reported in some cancer types [23]. Compared with C0-CD8-Tex T cells, C14-CD8-STMN1 T cells expressed intermediated levels of PDCD1,

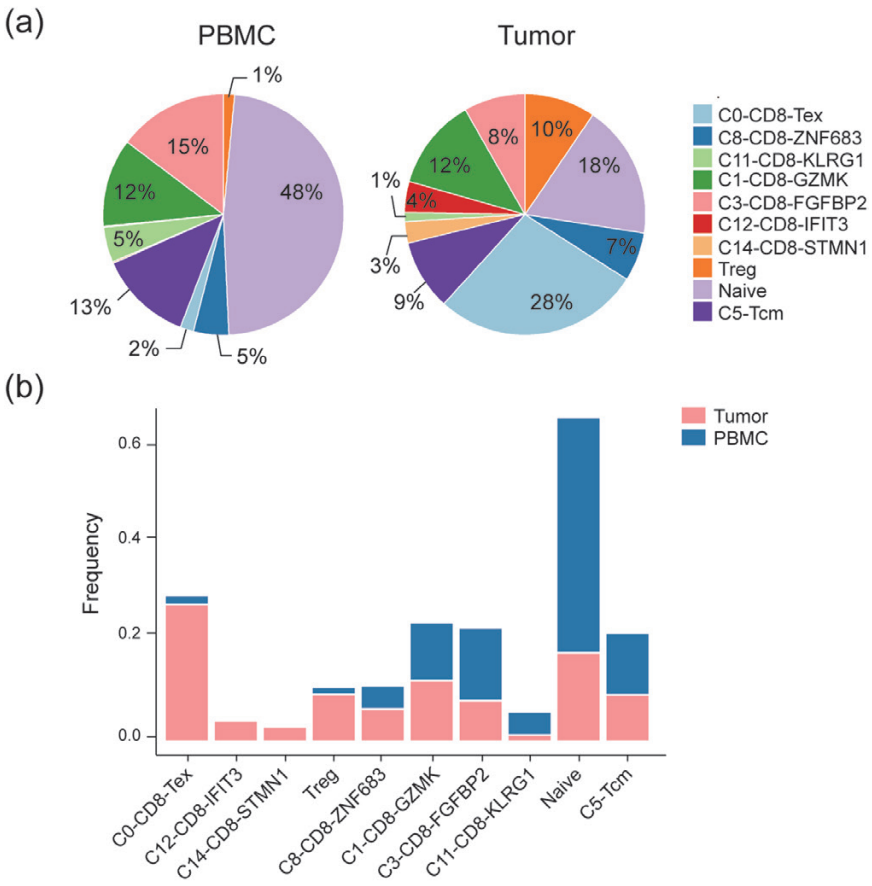

Figure 2. Profiles of T-cell compositions in human ESCC tumors and PBMCs. (a) Pie charts of T-cell subtype fractions for ESCC tumor and PBMCs, colored by cell type. (b) Bar plot showing the proportion of T-cell subtypes that contributed to samples (tumor and PBMCs), colored by samples.

HAVCR2, and TIGIT, while exhausted C0-CD8-Tex T cells expressed high levels of these molecules. C14-CD8-STMN1 T cells exhibited sustained expression of certain effector molecules (e.g. GNLY and EFHD2) and retained their capacity to mount responses against tumor cells, indicating these cells were preexhausted T cells (Fig. 3d). To better understand the T-cell types (C0-CD8-Tex, C14-CD8-STMN1, and C12-CD8-IFIT3) exhibiting exhaustion signatures within tumors, we performed the pathway-enrichment analysis. Gene ontology (GO) analysis of C0-CD8-Tex cells indicated significant enrichment for T-cell activation, cell–cell adhesion, antigen processing and presentation, immunoglobulin-mediated immune response, etc. (Fig. 3e). The GO terms enriched in this subcluster were all related to the development of $CD8^+$ T-cell exhaustion driven by antigen persistence [24]. GO analysis of C14-CD8-STMN1 T cells demonstrated significant enrichment for chromosome segregation, nuclear division, organelle fission, etc. (Fig. 3f), suggesting that these cells were extremely proliferative. By analyzing the cell cycle, we consistently showed that C14-CD8-STMN1 T cells had the highest G2M and S phase scores (Supplementary Fig. 2a and b), suggesting preexhausted T cells are the primary proliferating T-cell compartment in TME. In addition, the GO terms for C12-CD8-IFIT3 T cells were related to response to the virus, cytokine-mediated signaling pathway, response to interferon-beta and gamma, etc. (Fig. 3g), indicating that this subcluster was engaged in an interferon-mediated immune response. In summary, our data found that most of the tumor-infiltrating $CD8^+$ T cells were in the exhausted states in ESCC. In contrast, T cells in PBMCs were enriched in cytotoxic and naïve signatures. The enrichment of exhausted and suppressive T cells in ESCC tumors may contribute to the progression of the disease.

LAIR2 expression pattern in T cells of tumor and PBMCs

Previous data supported supplemental LAIR2 as a therapeutic intervention that might inhibit LAIR1 inhibitory interaction with collagen in the TME of solid tumors [13, 14]. However, its expression pattern and functional features have not been well studied. This study revealed that LAIR2 exhibited a particular expression pattern in C3-CD8-FGFBP2, C14-CD8-STMN1, and Treg cells (Fig. 4a). After deciphering the cell composition within the ESCC tumors and matched PBMCs, we found that LAIR2 was significantly enriched in C3-CD8-FGFBP2 T cells in PBMCs, while it was increased in C14-CD8-STMN1 and Treg cells in the tumors (Fig. 4b–g). The distinct expression pattern of LAIR2 in PBMCs and tumors implies its potential multifaceted role in modulating antitumor immunity. To better understand the transcriptional profiles of LAIR2 highly expressing T cells, we further determined differential expression genes (DEGs) of C3-CD8-FGFBP2, C14-CD8-STMN1, and Treg cells between PBMCs and tumors. The numbers of DEGs are shown in Supplementary Fig. 2c. C3-CD8-FGFBP2 and Treg cells showed much higher DEGs than C14-CD8-STMN1, indicating that the former two T-cell subtypes were more tissue-specific than C14-CD8-STMN1. Then, GO and GSEA pathway enrichment analyses were

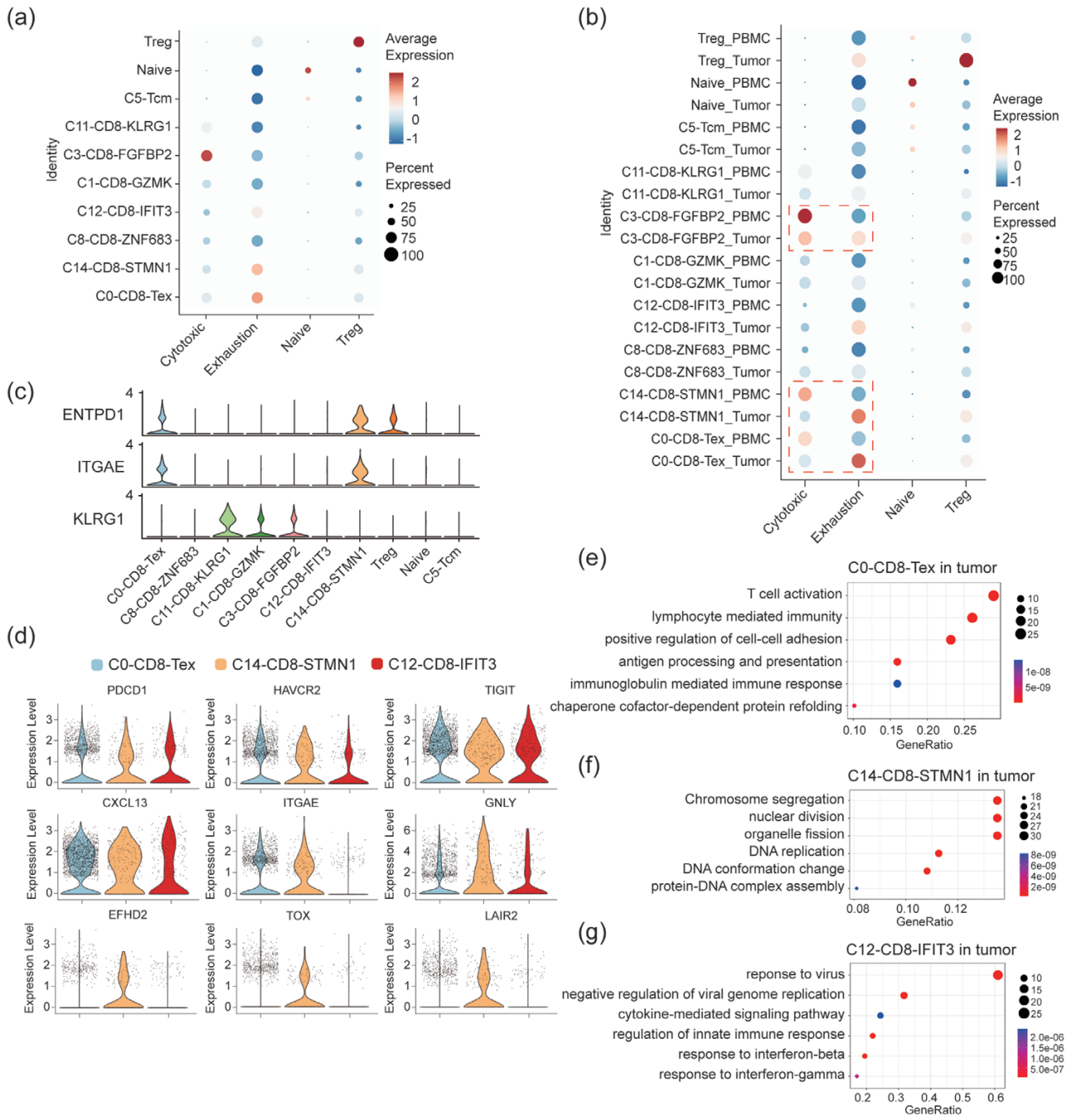

Figure 3. Detailed characterization of T cells in ESCC tumors and PBMCs. (a, b) Dot plot of representative cytotoxic, exhaustive, naïve, and Treg signatures in T-cell subtypes, *z*-score normalized log2(count + 1). (c) Violin plot showing ENTPD1, ITGAE, and KLRG1 expressions in T-cell subtypes in tumors and PBMCs. (d) Violin plot showing PDCD1, HAVCR2, TIGIT, CXCL13, ITGAE GNLY, EFHD2, TOX, and LAIR2 in the C0-CD8-Tex, C14-CD8-STMN1, and C12-CD8-IFIT3 T-cell clusters from ESCC tumors and PBMCs. The expression was measured as the log2(count+1). (e–g) Gene ontology (GO) enrichment analysis using the DEGs in T-cell subclusters in tumors.

conducted to explore the function of the upregulated DEGs in tumors compared with those in PBMCs. Notably, nearly all LAIR2 expressing T cells in tumors upregulated the expression of genes involved in "T-cell activation," "ATP synthesis coupled proton transport," "ATP metabolic process," and "energy coupled proton transport" biological process pathways (Fig. 4h). The GSEA analysis revealed that the genes in LAIR2 expressing T cells were significantly enriched in "TNF-α signaling via NF-κB," "Interferon-γ response," and "IL2-STAT5 signaling" pathways in tumors (Fig. 4i). These observations suggested that LAIR2 expressing T cells in tumors were highly activated, cytokine responsive, and had higher energy demands.

LAIR2 expression associated with cytotoxic activity

LAIR2 is a secreted receptor and functions as a natural competitor for LAIR1 [14]. In our data, LAIR2 had a very well-defined expression feature and showed a different expression pattern between tumors and PBMCs. To resolve the function of LAIR2 in ESCC progression, we treated ESCC cell

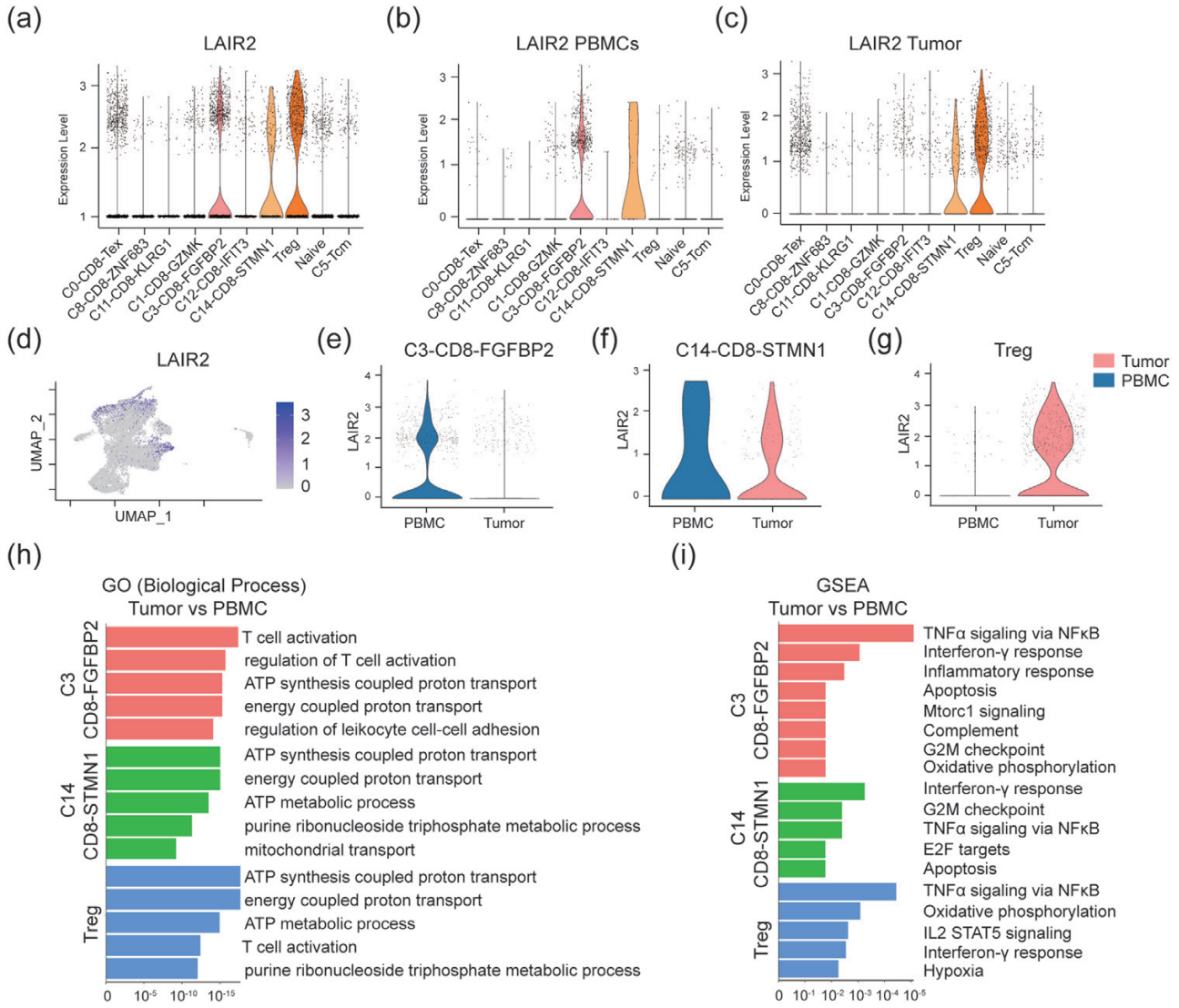

Figure 4. Characterization of LAIR2 expression in ESCC tumors and PBMCs. (a–c) Violin plot showing LAIR2 expression level in T-cell subtypes. (d) Expression level of LAIR2 across 16 538 cells was illustrated as UMAP plots. (e–g) Violin plot showing the LAIR2 expression level in three T-cell clusters in tumor and PBMCs. (h–i) GO enrichment and GSEA analysis using the genes upregulated in tumors compared with PBMCs.

line KYSE150 with varying concentrations of LAIR2 and measured tumor growth *in vitro*. As shown in Fig. 5a and b, cell growth and foci formation assays demonstrated that LAIR2 did not affect cell growth and proliferation. Notably, wound healing and transwell assays indicated that LAIR2 treatment significantly inhibited tumor motility and invasion in a concentration-dependent manner (Fig. 5c and d). These data showed that LAIR2 exerted a suppressive effect on nondirectional migration. In addition, our findings suggested that LAIR2 had an inhibitory effect on directional migration, as demonstrated by the results of the CXCL12 chemotaxis assay (Supplementary Fig. 3a and b). Epithelial–mesenchymal transition (EMT) strongly enhanced tumor motility and metastasis. One of the well-known growth factors to induce EMT is TGF-β [25]. We used a TGF-β-induced EMT model to investigate whether LAIR2 was involved in TGF-β-induced EMT. The wound healing assay showed that LAIR2-treated cells had slowed closure of the scratched "wound" compared with the control cells (Fig. 6a). Next, we analyzed the typical EMT-associated gene expressions. Q-PCR analysis demonstrated that LAIR2 treatment could upregulate the expression of E-cadherin in the presence or absence of TGF-β1. Meanwhile, LAIR2 could significantly downregulate N-cadherin, Vimentin, SNAIL2, and TWIST1 expressions in the presence of TGF-β1 (Fig. 6c). By calculating the grayscale value of E-cadherin, N-cadherin, SNAIL, and Vimentin with western blot, we demonstrated that LAIR2 could downregulate N-cadherin and SNAIL expressions in the presence and absence of TGF-β1 (Fig. 6b). These results indicated that LAIR2 inhibited tumor cell migration and invasion by suppressing EMT-associated gene expressions. TGF-β induced EMT in both SMAD signaling-dependent and independent pathways. The non-Smad signal transduction proteins included Rho-like GTPases RAC and Rho, MAPK, and PI3K [26]. TGF-β-induced EMT is characterized by dramatic cytoskeletal structure and protein expression changes, which are essential for cancer cell metastasis and invasion. To investigate the mechanism by which LAIR2 modulates TGF-β-induced EMT, western blotting and qPCR were employed. Our data revealed that the expressions of ROCK1,

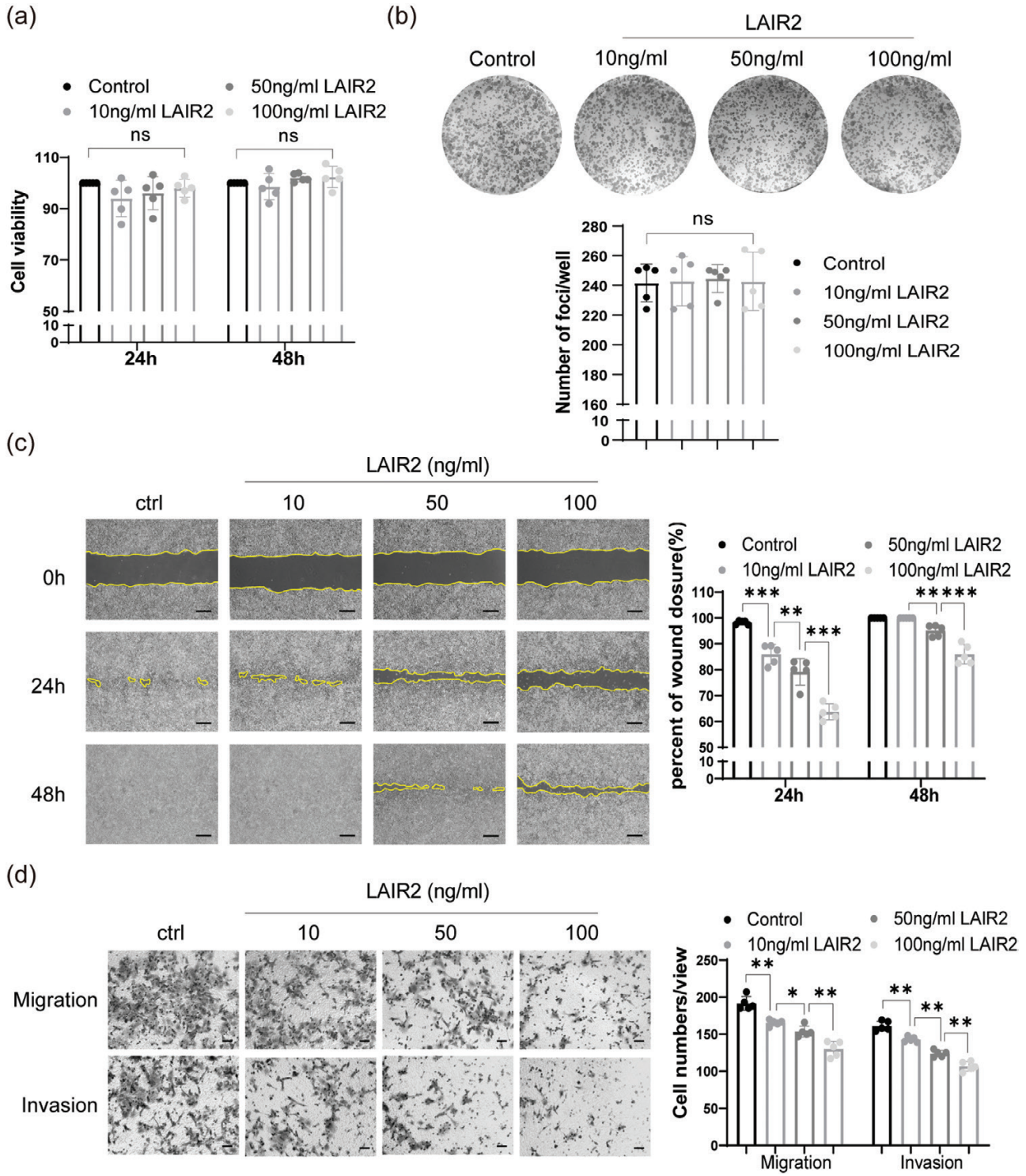

Figure 5. LAIR2 limited ESCC cell migration and invasion. (a–c) KYSE150 cells were cultured with different concentrations of LAIR2 protein for indicated time points. CCK8 cell growth assay (a) and foci formation analysis (b) were performed. The wound healing assay was carried out, and the wound area was calculated using ImageJ software. Scale bars = 1 mm (c). (d) KYSE150 cells were treated with indicated concentrations of LAIR2 protein for 48 hours. The transwell migration and invasion assays were conducted. Scale bars = 50 μm. Data from one representative experiment of three independent experiments were presented as the mean ± SD, $^{*}P < 0.05$, $^{**}P < 0.01$, $^{***}P < 0.001$, ns: no statistical significance.

p-Smad2/3, and p-AKT were downregulated upon treatment with LAIR2, both in the presence and absence of TGF-β1 (Fig. 6d). LAIR2 treatment effectively downregulated collagen expression and inhibited NF-κB and LEF-1 activation both in the presence and absence of TGF-β1 (Supplementary Fig. 4a and c). However, it was observed that LAIR2 treatment failed to inhibit LEF-1 and NF-κB expressions in the presence of collagen I (Supplementary Fig. 4b), indicating that LAIR2 did not exert any effect on the activation on ILK pathway induced by collagen. In addition, we applied immunofluorescences to

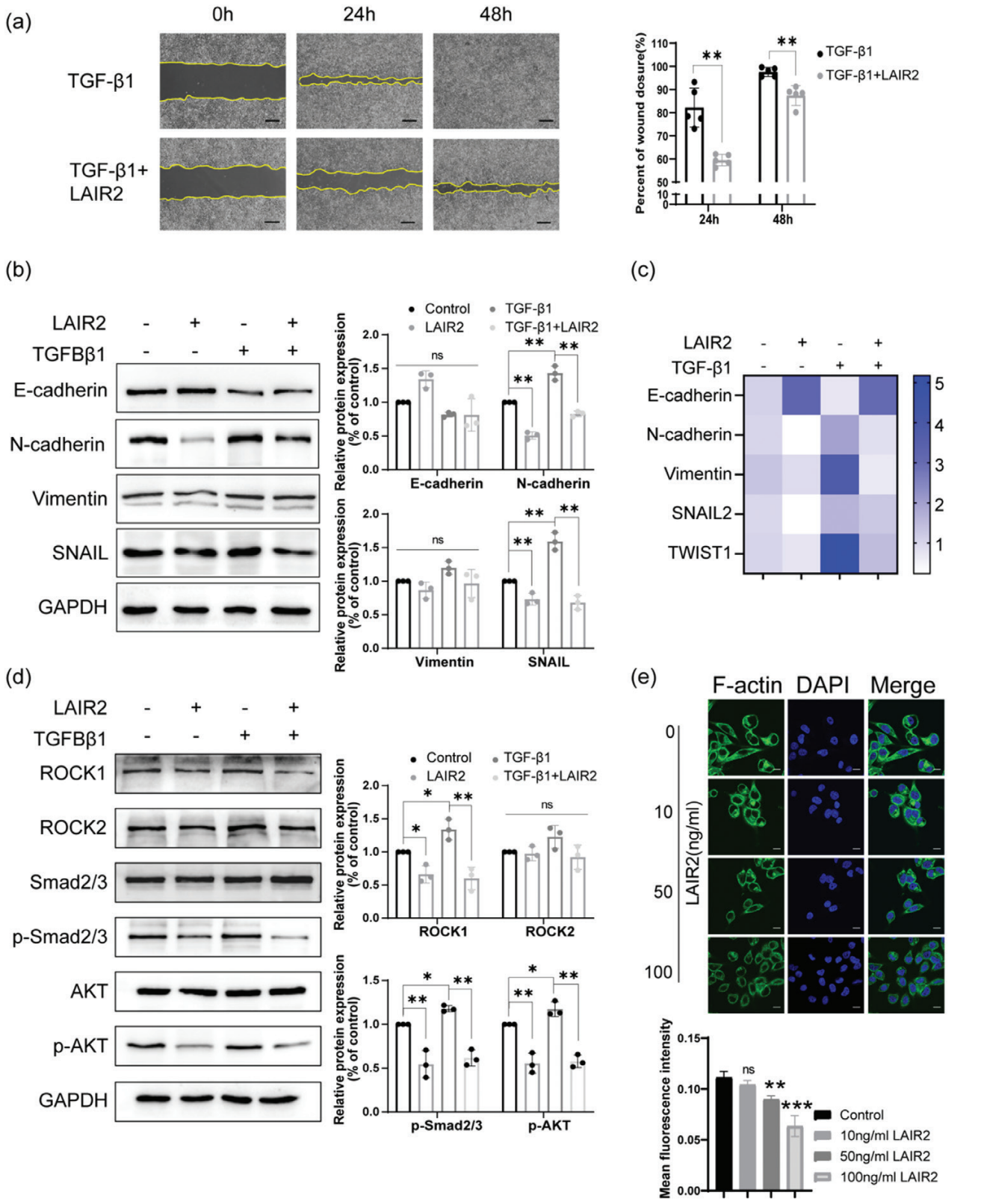

Figure 6. LAIR2 suppressed the EMT process of ESCC tumor cells. (a) KYSE150 cells were cultured with 10 ng/mL TGF-β1 in the presence or absence of 100 ng/mL LAIR2 for indicated time points. The wound healing process was assessed. Scale bars = 1mm. (b–d) KYSE150 cells were cultured with 10 ng/mL TGF-β1 in the presence or absence of 100 ng/mL LAIR2 for 48 hours. (b) The protein levels of E-cadherin, N-cadherin, Vimentin, and SNAIL were determined by western blotting. (c) The mRNA levels of E-cadherin, N-cadherin, Vimentin, SNAIL2, and TWIST1 were determined by RT-PCR analysis ($n = 3$). (d) Total or phosphorylated levels of ROCK1, ROCK2, Smad2/3, and AKT were evaluated by western blotting. (e) The effect of LAIR2 to the expression of F-actin in KYSE150 cells was examined by immunofluorescent staining. Scale bars = 10 μm. Data from one representative experiment of three independent experiments were presented as the mean ± SD, $^{*}P < 0.05$, $^{**}P < 0.01$, $^{***}P < 0.001$, ns: no statistical significance.

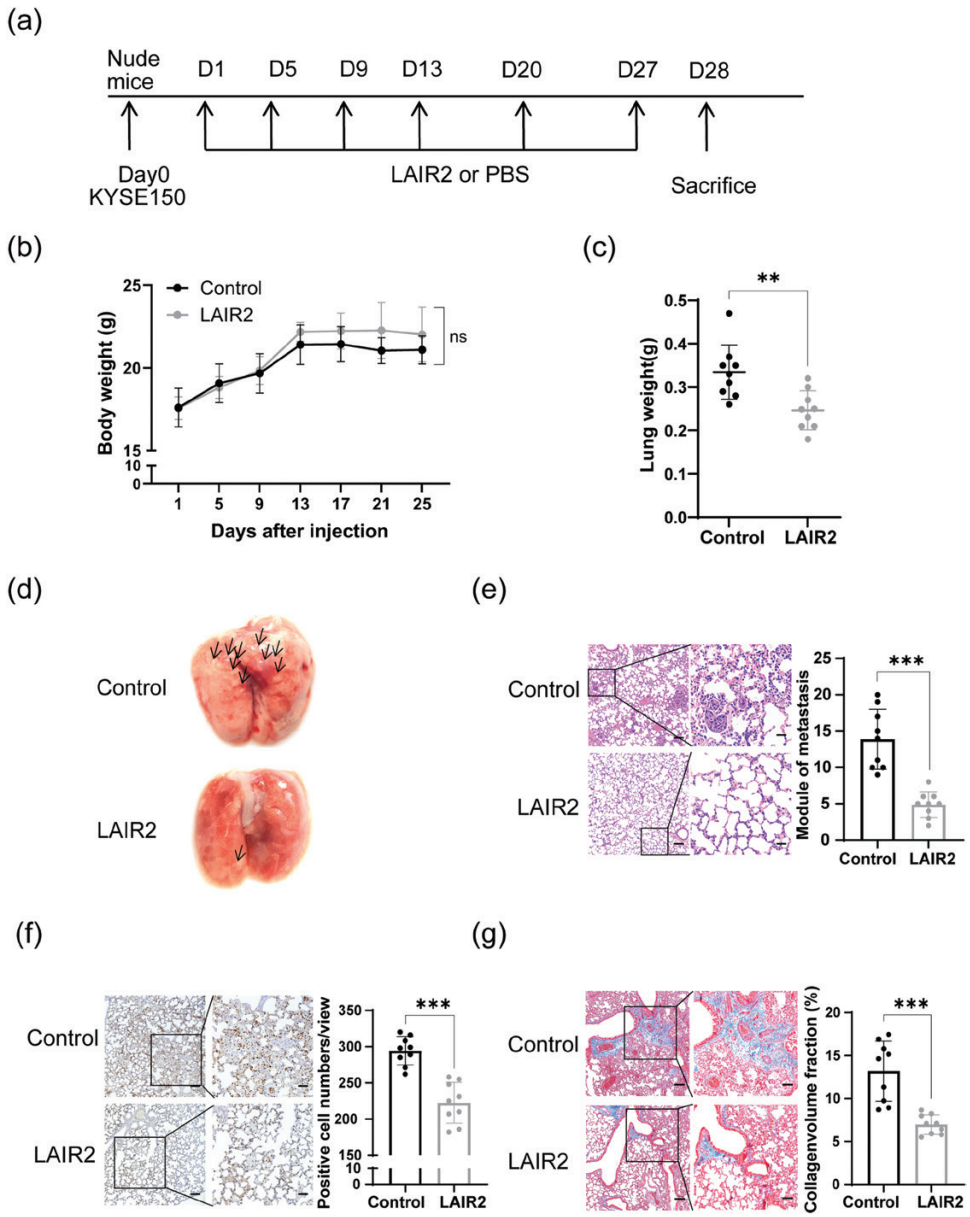

Figure 7. LAIR2 prevented tumor metastasis *in vivo*. (a) Five-week-old male nude mice were injected with 1 10^6 KYSE150 cells through the tail vein. After injection, mice were randomly divided into two groups. The mice were treated with 6 μg/kg LAIR2 or PBS by intraperitoneal injection until the endpoint (n = 10). (b) Weights of mice were recorded after LAIR2 injection. (c) Lung weights of mice were recorded at the endpoint. (d, e) The lung tissue and H&E staining analysis were performed, and the metastasis nodules were calculated. Scale bars (left) = 100 μm, scale bars (right) = 25 μm. (f) Ki67 immunohistochemistry staining of lung tissues was presented, and the positive cells were counted for statistical analysis. Scale bars (left) = 50 μm, scale bars (right) = 25 μm. (g) Masson Trichrome staining of lung tissues was presented. Collagen volume fraction was acquired through ImageJ software. Scale bars (left) = 50 μm, scale bars (right) = 25 μm. Data from one representative experiment from at least three independent experiments were presented as the mean ± SD, *P < 0.05, **P < 0.01, ***P < 0.001, ns: no statistical significance.

visualize cellular F-actin structure and expression. LAIR2 treatment significantly reduced F-actin cytoskeleton abundance (Fig. 6e). Furthermore, we observed that F-actin expression induced by CXCL12 could be inhibited by LAIR2 stimulation, as shown in Supplementary Fig. 3c. These data indicated that LAIR2 potentially inhibited EMT through Smad-dependent and Sm ad-independent ways, as well as regulating cytoskeletal organization, ultimately leading to the inhibition of cell migration and invasion in ESCC tumor cells.

In this study, we used a mouse pulmonary metastasis model to investigate the effect of LAIR2 on tumor cell metastasis *in vivo*. Specially, we injected 1 × 10^6 KYSE150 cells through tail veins of male nude mice, which were randomly assigned to either the LAIR2 treatment or the control group (n = 10 in each group). Intraperitoneal injection of LAIR2 or PBS was administered accordingly (Fig. 7a). The body weights of the mice did not show significant differences between the two groups (Fig. 7b). However, the LAIR2-treated mice demonstrated markedly reduced lung weights (Fig. 7c). After a period of 28 days, the mice were sacrificed, and the pulmonary metastatic nodules were analyzed. The LAIR2 treatment group exhibited a marked decrease in pulmonary metastatic nodules compared with the control group (Fig. 7d). Furthermore, the H&E staining analysis revealed a decrease

in metastatic nodules in tumor-bearing mice upon LAIR2 treatment (Fig. 7e). These findings suggest that LAIR2 significantly reduces tumor cell metastasis *in vivo*. In addition, immunohistochemistry staining of Ki-67 demonstrated that LAIR2 treatment suppressed tumor cell proliferation *in vivo* (Fig. 7f), which was not observed *in vitro* study. Moreover, LAIR2 downregulated the percentage of PD-1$^+$TIM-3$^+$CD8$^+$ exhausted T cells *in vitro* (Supplementary Fig. 4d) and PD-L1 expressions on tumor cells *in vivo* (Supplementary Fig. 4e and f). These results indicate that T-cell-derived LAIR2 plays a role in antitumor immunity. Considering LAIR2 acts as a decoy receptor by binding collagen with a higher affinity than LAIR1 [13], we applied Masson Trichrome staining to detect collagen expression in lung tissues. We observed that LAIR2 treatment reduced collagen deposition in lung tissue (Fig. 7g). Collectively, these data demonstrate that LAIR2 acts as a tumor suppressor by inhibiting tumor metastasis and proliferation *in vivo*.

Discussion

In our previous study, we have described a detailed T-cell landscape of ESCC infiltrated T cells [27]. In the present study, we included 7815 T cells from matched PBMCs and tried to deciphered the differences of T-cell compositions between tumor and PBMCs. Indeed, we observed significant differences in the proportion of T-cell subpopulations between tumors and PBMCs. Specifically, we noted ESCC tumors were significantly enriched in exhausted T cells (C0-CD8-Tex), proliferating T cells (C14-CD8-STMN1), and Treg cells (C7-Tregs). However, PBMCs were significantly enriched in cytotoxic (C3-CD8-FGFBP2 and C11-CD8-KLRG1) and naïve T cells. The heterogenous T-cell compositions between tumor and PBMCs suggested an immunosuppressive network in tumor that could promote tumor growth and attenuate immune attack. Both exhausted T cells (C0-CD8-Tex) and proliferating T cells (C14-CD8-STMN1) in tumors expressed cytotoxic molecules (e.g. NKG7, GZMA, and GNLY) and exhausted signatures (e.g. PDCD1, HAVCR2 and LAG3), and they were the targets of immune checkpoint inhibitors reversing T-cell exhaustion [24]. Besides the heterogenous T-cell compositions in tumors and PBMCs, we also determined that T-cell subtypes had different cytotoxic and exhausted signatures between tumors and PBMCs. It was found that the genes related to persistence of antigen stimulation were highly expressed in C0-CD8-exhausted T cells in tumors. And the cytotoxic signatures of cytotoxic T cells (C3-CD8-FGFBP2) were much higher in PBMCs rather than in tumors. Therefore, our data suggested an immune suppressive environment and a persistent antigen stimulation that driven T-cell exhaustion in TME.

After dissecting T-cell compositions and profiling their transcriptomes in tumors and PBMCs, we focused on LAIR2, a secreted receptor that shares a similar extracellular domain with LAIR1. LAIR1 is a collagen-receptor that inhibits immune cell function through SHP-1 signaling upon collagen binding [13]. Acting as a decoy receptor of LAIR1, LAIR2 has been reported to show immune regulatory function. Former studies have shown that LAIR2 expression was elevated in systemic autoimmune diseases (e.g. rheumatoid arthritis, systemic lupus erythematosus, pemphigus vulgaris, and ankylosing spondylitis), suggesting a role for LAIR2 in regulating autoimmune disorders and inflammatory responses [16, 28–30]. In tumor immunity, LAIR2 overexpression has been implicated in rescuing exhaustive CD8$^+$ T cells and promoting immune infiltration in lung cancer by competitive binding with LAIR1 [14]. The other study revealed that the LAIR2 Fc fusion protein acted as a novel immune medicine to target tumor ECM and promote T-cell function through LAIR1 blockade [15]. However, controversial results based on the TCGA database and single-cell dataset reported that LAIR2 was expressed by Treg cells and partial GZMB$^+$ CD8$^+$ T cells in cholangiocarcinoma. They concluded that LAIR2 was a potential marker for exhaustive T-cell populations, correlating with the worse survival of patients [31]. We analyzed T-cell transcriptomes and found that LAIR1 was detected at low levels in each T-cell subcluster (Supplementary Fig. 1f). LAIR2 was highly expressed in cytotoxic CD8T cells (C3-CD8-FGFBP2) in PBMCs, while it was highly expressed in proliferating CD8T cells (C14-CD8-STMN1) and Treg cells in tumors. This signified a complicated role of LAIR2 in regulating antitumor immunity, and it remains to be investigated.

In our *in vitro* experiments, we found that LAIR2 inhibited tumor metastasis and invasion but had no effect on tumor growth or proliferation, suggesting a role of LAIR2 in EMT suppression. EMT is a crucial process in cancer metastasis. During EMT, the epithelial characteristics and integrity are lost, whereas the expression of the mesenchymal cell–cell adhesion molecule N-cadherin is induced [32]. TGF-β is probably the most potent inducer of the EMT process. TGF-β interaction with its receptors triggered signal transduction in Smad-dependent and independent ways to exert its function. The non-Smad signal transduction includes RHO-like GTPases (i.e. RAC and RHO), MAPK, and phosphoinositide 3-kinase (PI3K) pathways [26]. In our data, LAIR2 significantly inhibited N-cadherin expression in the presence or absence of TGF-β. Meanwhile, LAIR2 suppressed the phosphorylation of both Smad3 and AKT, indicating that LAIR2 could inhibit both Smad-dependent and nondependent TGF-β signaling activation, thereby inhibiting the TGF-β-induced EMT process.

Cancer cell metastasis is a multistage process involving the invasion of surrounding tissue. Many of these steps require cell motility, which is dependent on the dynamic remodeling of the actin cytoskeleton and the formation of invasive structures [33, 34]. F-actin is a long-chain polar polymer formed due to the polymerization of globular actin (G-actin). Previous studies found that F-actin was positively correlated with HER-2 expression and lymph node metastasis in breast cancer [35]. We demonstrated that LAIR2 treatment significantly reduced the F-actin level in ESCC tumor cells. Collagen is the most abundant component of the ECM, contributing to the stability and integrity of tissues. In many tumors, increased collagen expression, density, and organization have been associated with poor prognosis [36]. Collagen fragments in TME can directly interact with the inhibitory collagen receptor LAIR1. A previous study has shown that Fc fusion proteins of LAIR2 have the potential as cancer immunotherapeutic agents by acting as a LAIR1 decoy receptor [15]. In our *in vivo* study, administration of LAIR2 protein could significantly downregulate tumor metastasis and collagen deposition in lung tissue in nude mice. In addition, our results showed that LAIR2 downregulated the percentage of PD-1$^+$ TIM-3$^+$ CD8$^+$ exhausted T cells *in vitro* and PD-L1 expressions on tumor cells, which were

consistent with previous findings that over expression of LAIR2 could sensitize lung tumors to PD-1 blockade [15], indicating that LAIR2 could reduce tumor immune escape. We now consider that LAIR2 directly inhibits tumor metastasis and invasion which might be carried out in a LAIR1-independent manner. And its immunosuppressive effect provided more convincing evidence that LAIR2 acted as a tumor suppressor.

In summary, our transcriptional map of T cells from ESCC tumors and matched PBMCs provided a picture for understanding the adaptive immune status. In addition, we illustrated the LAIR2 expression pattern and function. Our findings also complement the role and mechanism of LAIR2 in antitumor immunity, which are essential for developing immunotherapies in ESCC.

Supplementary data

Supplementary data is available at *Clinical and Experimental Immunology* online.

Ethical approval

Human samples

All samples were obtained from patient who had previously signed an informed consent. The collection of all the samples were approved by the Committees for the Ethical Review of Research Involving Human Subjects at the Sun Yat-sen University Cancer Center (Guangzhou, Guangdong, P.R. China).

Animal studies

All animal experiments were approved by the Welfare and Ethical Committee for Experimental Animal Care of Southern Medical University (2020066).

Conflict of interests

None declared.

Funding

This work was supported by the National Natural Science Foundation of China (82173083) and Natural Science Foundation of Guangdong Province (2022A1515012579).

Data availability

All data needed to evaluate the conclusions in the paper are present in the paper and/or the supplementary material. The data used to support the findings of this study are included within the article.

Author contributions

Q.C. and X.Z. designed the research. P.W., W.Z., Z.Z., and L.Z. conceived the experiments and performed the data analysis. Y.L., P.W., W.Z., and Q.C. analyzed the data. P.W. and Q.C. wrote and revised the manuscript with input from all coauthors.

Permission to reproduce

Not applicable.

References

1. Rustgi AK, El-Serag HB. Esophageal carcinoma. *N Engl J Med* 2014, 371, 2499–509. doi:10.1056/NEJMra1314530.
2. Liu J, Xie X, Zhou C, Peng S, Rao D, Fu J. Which factors are associated with actual 5-year survival of oesophageal squamous cell carcinoma?. *Eur J Cardiothorac Surg* 2012, 41, e7–11. doi:10.1093/ejcts/ezr240.
3. Huang TX, Fu L. The immune landscape of esophageal cancer. *Cancer Commun (Lond)* 2019, 39, 79. doi:10.1186/s40880-019-0427-z.
4. Shitara K, Özgüroğlu M, Bang YJ, Di Bartolomeo M, Mandalà M, Ryu MH, et al.. Pembrolizumab versus paclitaxel for previously treated, advanced gastric or gastro-oesophageal junction cancer (KEYNOTE-061): a randomised, open-label, controlled, phase 3 trial. *Lancet (London, England)* 2018, 392, 123–33. doi:10.1016/S0140-6736(18)31257-1.
5. Zhang X, Peng L, Luo Y, Zhang S, Pu Y, Chen Y, et al. Dissecting esophageal squamous-cell carcinoma ecosystem by single-cell transcriptomic analysis. *Nat Commun* 2021, 12, 5291. doi:10.1038/s41467-021-25539-x.
6. Sathish JG, Johnson KG, Fuller KJ, LeRoy FG, Meyaard L, Sims MJ, et al. Constitutive association of SHP-1 with leukocyte-associated Ig-like receptor-1 in human T cells. *J Immunol (Baltimore, Md: 1950)* 2001, 166, 1763–70.
7. Nissen NI, Karsdal M, Willumsen N. Collagens and cancer associated fibroblasts in the reactive stroma and its relation to Cancer biology. *J Exp Clin Cancer Res* 2019, 38, 115.
8. LAIR-1, a novel inhibitory receptor expressed on human mononuclear leukocytes. *Immunity* 1997, 7, 283–90.
9. Jansen CA, Cruijsen CW, de Ruiter T, Nanlohy N, Willems N, Janssens-Korpela PL, et al. Regulated expression of the inhibitory receptor LAIR-1 on human peripheral T cells during T cell activation and differentiation. *Eur J Immunol* 2007, 37, 914–24. doi:10.1002/eji.200636678.
10. Merlo A, Tenca C, Fais F, Battini L, Ciccone E, Grossi CE, et al. Inhibitory receptors CD85j, LAIR-1, and CD152 down-regulate immunoglobulin and cytokine production by human B lymphocytes. *Clin Diagn Lab Immunol* 2005, 12, 705–12. doi:10.1128/CDLI.12.6.705-712.2005.
11. Son M, Diamond B. C1q-mediated repression of human monocytes is regulated by leukocyte-associated Ig-like receptor 1 (LAIR-1). *Mol Med* 2015, 20, 559–68. doi:10.2119/molmed.2014.00185.
12. Lebbink RJ, de Ruiter T, Adelmeijer J, Brenkman AB, van Helvoort JM, Koch M, et al. Collagens are functional, high affinity ligands for the inhibitory immune receptor LAIR-1. *J Exp Med* 2006, 203, 1419–25. doi:10.1084/jem.20052554.
13. Lebbink RJ, van den Berg MC, de Ruiter T, Raynal N, van Roon JA, Lenting PJ, et al. The soluble leukocyte-associated Ig-like receptor (LAIR)-2 antagonizes the collagen/LAIR-1 inhibitory immune interaction. *J Immunol (Baltimore, Md: 1950)* 2008, 180, 1662–9.
14. Peng DH, Rodriguez BL, Diao L, Chen L, Wang J, Byers LA, et al. Collagen promotes anti-PD-1/PD-L1 resistance in cancer through LAIR1-dependent CD8(+) T cell exhaustion. *Nat Commun* 2020, 11, 4520.
15. Ramos MIP, Tian L, de Ruiter EJ, Song C, Paucarmayta A, Singh A, et al. Cancer immunotherapy by NC410, a LAIR-2 Fc protein blocking human LAIR-collagen interaction. *Elife* 2021, 10, e62927.
16. Olde Nordkamp MJ, van Roon JA, Douwes M, de Ruiter T, Urbanus RT, Meyaard L. Enhanced secretion of leukocyte-associated immunoglobulin-like receptor 2 (LAIR-2) and soluble LAIR-1 in rheumatoid arthritis: LAIR-2 is a more efficient antagonist of the LAIR-1-collagen inhibitory interaction than is soluble LAIR-1. *Arthritis Rheum* 2011, 63, 3749–57. doi:10.1002/art.30612.
17. Ly D, Li Q, Navab R, Zeltz C, Fang L, Cabanero M, et al. Tumor-associated regulatory T cell expression of LAIR2 is prognostic in lung adenocarcinoma. *Cancers (Basel)* 2021, 14, 205.
18. Zheng Y, Chen Z, Han Y, Han L, Zou X, Zhou B, et al. Immune suppressive landscape in the human esophageal squamous cell

carcinoma microenvironment. *Nat Commun* 2020, 11, 6268. doi:10.1038/s41467-020-20019-0.
19. Savas P, Virassamy B, Ye C, Salim A, Mintoff CP, Caramia F, et al. Single-cell profiling of breast cancer T cells reveals a tissue-resident memory subset associated with improved prognosis. *Nat Med* 2018, 24, 986–93.
20. Inflammation directs memory precursor and short-lived effector CD8(+) T cell fates via the graded expression of T-bet transcription factor. *Immunity* 2007, 27, 281–95.
21. Guo X, Zhang Y, Zheng L, Zheng C, Song J, Zhang Q, et al. Global characterization of T cells in non-small-cell lung cancer by single-cell sequencing. *Nat Med* 2018, 24, 978–85. doi:10.1038/s41591-018-0045-3.
22. Duhen T, Duhen R, Montler R, Moses J, Moudgil T, de Miranda NF, et al. Co-expression of CD39 and CD103 identifies tumor-reactive CD8 T cells in human solid tumors. *Nat Commun* 2018, 9, 2724. doi:10.1038/s41467-018-05072-0.
23. Kurachi M. CD8(+) T cell exhaustion. *Semin Immunopathol* 2019, 41, 327–37. doi:10.1007/s00281-019-00744-5.
24. Blank CU, Haining WN, Held W, Hogan PG, Kallies A, Lugli E, et al. Defining 'T cell exhaustion'. *Nat Rev Immunol* 2019, 19, 665–74. doi:10.1038/s41577-019-0221-9.
25. Xie F, Ling L, van Dam H, Zhou F, Zhang L. TGF-beta signaling in cancer metastasis. *Acta Biochim Biophys Sin (Shanghai)* 2018, 50, 121–32. doi:10.1093/abbs/gmx123.
26. Derynck R, Zhang YE. Smad-dependent and Smad-independent pathways in TGF-beta family signalling. *Nature* 2003, 425, 577–84. doi:10.1038/nature02006.
27. Chen QY, Li YN, Wang XY, Zhang X, Hu Y, Li L, et al. Tumor fibroblast-derived FGF2 regulates expression of SPRY1 in esophageal tumor-infiltrating T cells and plays a role in T-cell exhaustion. *Cancer Res* 2020, 80, 5583–96. doi:10.1158/0008-5472.CAN-20-1542.
28. Simone R, Pesce G, Antola P, Merlo DF, Bagnasco M, Saverino D. Serum LAIR-2 is increased in autoimmune thyroid diseases. *PLoS One* 2013, 8, e63282. doi:10.1371/journal.pone.0063282.
29. Camargo CM, Augusto DG, Petzl-Erler ML. Differential gene expression levels might explain association of LAIR2 polymorphisms with pemphigus. *Hum Genet* 2016, 135, 233–44. doi:10.1007/s00439-015-1626-6.
30. Farias TDJ, Augusto DG, de Almeida RC, Malheiros D, Petzl-Erler ML. Screening the full leucocyte receptor complex genomic region revealed associations with pemphigus that might be explained by gene regulation. *Immunology* 2019, 156, 86–93. doi:10.1111/imm.13003.
31. Chen Z, Yu M, Yan J, Guo L, Zhang B, Liu S, et al. PNOC expressed by B cells in cholangiocarcinoma was survival related and LAIR2 could be a T cell exhaustion biomarker in tumor microenvironment: characterization of immune microenvironment combining single-cell and bulk sequencing technology. *Front Immunol* 2021, 12, 647209. doi:10.3389/fimmu.2021.647209.
32. Brabletz S, Schuhwerk H, Brabletz T, Stemmler MP. Dynamic EMT: a multi-tool for tumor progression. *EMBO J* 2021, 40, e108647. doi:10.15252/embj.2021108647.
33. Best M, Gale ME, Wells CM. PAK-dependent regulation of actin dynamics in breast cancer cells. *Int J Biochem Cell Biol* 2022, 146, 106207. doi:10.1016/j.biocel.2022.106207.
34. Yang L. TGFbeta and cancer metastasis: an inflammation link. *Cancer Metastasis Rev* 2010, 29, 263–71. doi:10.1007/s10555-010-9226-3.
35. Shao J, Zhang H, Wang Z. Coronin 1c and F-actin promote metastasis of breast cancer. *Med Sci Monit* 2018, 24, 5980–7. doi:10.12659/MSM.908929.
36. Provenzano PP, Inman DR, Eliceiri KW, Knittel JG, Yan L, Rueden CT, et al. Collagen density promotes mammary tumor initiation and progression. *BMC Med* 2008, 6, 11. doi:10.1186/1741-7015-6-11.